A comprehensive study of the high temperature pyrolysis of sewage sludge: kinetics, energy analysis and products formation

Mendoza-Geney L.*, Rincón Prat S. and Gómez A.

Universidad Nacional de Colombia - sede Bogotá - Facultad de Ingeniería - Departamento de Ingeniería Mecánica y Mecatrónica - Grupo de Investigación en Biomasa y Optimización Térmica de Procesos - Carrera 30 No 45A-03 Edificio 453 Of. 400, Bogotá, Colombia
*to whom all correspondence should be addressed: e-mail: lemendozag@unal.edu.co

Graphical abstract
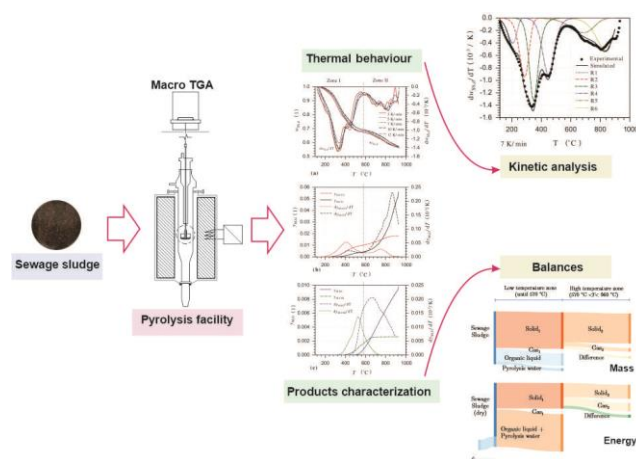
Abstract

This study evaluates the pyrolysis of sewage sludge until 960°C using heating rates between 3 K/min and 12 K/min in a macro TG/EGA. Mass and energy balances and kinetic parameters are determined. Thermal decomposition is divided into a low temperature zone (until 550°C to 590°C), for decomposition of organic matter, and a high temperature zone, for decomposition of inorganic matter and secondary reactions of the residual organic matter. In dry basis at 570°C solid, liquid and gaseous products amount to 69.2 wt%, 29.2 wt% and 1.6 wt%, respectively. An increment in the final temperature to 960°C causes a successive decrease of the solid residue to 56.9 wt%. The solid product contains more than 80 wt% mineral matter with high amounts of valuable elements, such as calcium (Ca) and phosphorus (P). An energy requirement of 2.18 MJ/kg of dry sewage sludge is calculated for the pyrolysis until 570°C. At this temperature, 58.5% of the energy entering the process is concentrated in the liquid product and 40.0% in the solid. A suitable set of kinetic parameters is determined through a formal independent parallel reactions model with six-pseudo components, using a combination of isoconversional and fitting methods.

Keywords: Pyrolysis, sewage sludge, thermogravimetry, kinetic modeling, mass and energy balances

1. Introduction

There are substantial benefits to be gained from thermochemical processing as an alternative route to sewage sludge disposal to landfill sites and soils. The composition of sewage sludge generated in wastewater treatment plants is complex and contains organic matter, pathogens, heavy metals, micropollutants and leachates (Kacprzak *et al.*, 2017), but also relevant fractions of nutrients such as phosphorus, calcium, potassium and sodium (Chanaka *et al.*, 2019b). Damages to the soil and water resources and risks to public health have led to increasing restrictions on the disposal of sewage sludge in landfills and soils worldwide (Kacprzak *et al.*, 2017). However, the costs associated with its treatment through thermochemical processes, such as incineration, are higher than traditional disposal methods, which are still widely used. Due to the increasing deployment of wastewater treatment in developing countries and the tightening of wastewater regulations (Wichelns *et al.*, 2015), an increase in global sewage sludge production is expected in the coming years. Moreover recent regulatory developments have encouraged the implementation of measures for the recovery of nutrients, especially phosphorus, present in sewage sludge (Bergfeldt *et al.*, 2018).

The pyrolysis of sewage sludge has the potential to achieve advantages similar to those offered by incineration, such as the reduction in the volume of residues, the elimination of harmful components, the possibility of energy and nutrients recovery, and other uses to the inorganic solid residues (Kacprzak *et al.*, 2017). The lower temperatures at which pyrolysis can be carried out, compared with incineration and gasification, offer operational advantages associated with the avoidance of heavy metals volatilization, dioxin and furans formation (Chanaka *et al.*, 2019b), and other problems related to ash melting, sintering and agglomeration (Seggiani *et al.*, 2012). The production of solid, liquid and gaseous products offers additional advantages for pyrolysis as a possible technical and ecological treatment of sewage sludge (Trinh *et al.*, 2013). In relation to the use of char

Mendoza-Geney L., Rincón Prat S. and Gómez A. (2021), A comprehensive study of the high temperature pyrolysis of sewage sludge: kinetics, energy analysis and products formation, *Global NEST Journal*, **23**(XX), 1-13.

from sewage sludge pyrolysis, several studies have shown that the leaching potential of heavy metals decreases in charcoal (Chanaka *et al.*, 2019b, Wesenbeeck *et al.*, 2014). It has also been reported that the extraction potential of phosphorus (P) for pyrolysis char is higher than that for combustion ash (Bergfeldt *et al.*, 2018). Compared with lignocellulosic biomass, sewage sludge adds the complexity of its composition as a decisive variable during pyrolysis. Typically, after a dewatering step, it has a water content between 65 wt% and 80 wt% (Roskosch and Heidecke, 2018). For thermal processing, water contents below 15 wt% are desired, so an additional drying step must be added before processing (Gao *et al.*, 2020). The dry matter of sewage sludge is composed of a fraction of organic matter that includes proteins, lipids, hemicellulose, cellulose and lignin (Thipkhunthod *et al.*, 2007; Zhu *et al.*, 2019), and by a fraction of inorganic matter, mainly silicates, oxides, sulphates and heavy metals Tang *et al.*, 2018. This last fraction varies from around 20 wt% to 54 wt% (dry basis) (Thipkhunthod *et al.*, 2007; Zhu *et al.*, 2019) and exerts a determining influence on the yield of the solid residue due to catalytic effects and decomposition reactions at high temperatures Shao *et al.*, 2010. The products distribution during sewage sludge pyrolysis is additionally influenced by the process parameters. Experimental pyrolysis studies are commonly performed until final temperatures between 450°C and 650°C. Product yields, in dry basis, vary in a wide interval with solid mass fractions in the range between 32 wt% (Gao *et al.*, 2014) and 78 wt% (Trinh *et al.*, 2013), liquid fractions between 14 wt% (Trinh *et al.*, 2013) and 48 wt% (Álvarez *et al.*, 2015), and gas fractions between 5 wt% (Álvarez *et al.*, 2015) and 40 wt% (Karaca *et al.*, 2018). Maximum liquid yields have been obtained between 500°C and 650°C. The effects of the heating rate are appreciable until the end of the pyrolysis reactions of the organic fraction. With an increase in the pyrolysis temperature from 450°C to 650°C and 850°C (Gao *et al.*, 2014; guanzo *et al.*, 2002) reported very small variations in the product yields with the heating rate. (Casajus *et al.*, 2009; Zhu *et al.*, 2019) obtained similar solid yields at different heating rates when using final pyrolysis temperatures of 900°C and 1000°C, respectively.

The high variability of sludge composition and its influence on pyrolysis also make it difficult to determine suitable reaction parameters for process development. Reaction kinetics has been mainly modeled using single-step global (Ji *et al.*, 2010), multiple-step (Casajus *et al.*, 2009) and semi-global (Calvo *et al.*, 1982; Calvo *et al.*, 2004; Font *et al.*, 2005; García *et al.*, 2009; Thipkhunthod *et al.*, 2007; Urban and Anta, 1982; Urych and Smolinski, 2016; Xu *et al.*, 2018) reaction models. Semi-global models of independent parallel reactions, according to pseudo-components decomposition, represent satisfactorily the thermal decomposition of sewage sludge. Table 1 presents a summary of relevant kinetic studies for the pyrolysis of sewage sludge using this type of models. The determination of the kinetic parameters is performed mostly using fitting procedures applied to experimental data. Isoconversional methods are also

applied in combination with a kinetic model. In these methods the activation energy is determined using experiments at different heating rates, thus avoiding the compensation effect between E_a and k_0 that can occur when applying only model-fitting (Anca *et al.*, 2014). In the works presented in Table 1, Urban and Antal 2982 applied the Friedmann isoconversional method, while (Urych and Smolinski, 2016) use a combination of deconvolution of experimental data and application of the Kissinger-Akahira-Sunose (KAS) isoconversional method of each obtained curve.

The present work evaluates the pyrolysis of sewage sludge samples obtained from the wastewater treatment plant of Bogotá (Colombia). The aims of the study are to give a qualitative insight into the behavior of organic and inorganic matter during thermal decomposition of the sewage sludge, to establish mass and energy balances and to determine a suitable set of kinetic reaction parameters of the process. Pyrolysis temperatures up to 960°C are used. A macro TG-facility with evolved gas analysis (EGA) is employed. A formal kinetic model of six parallel independent reactions is used to represent the mass loss of sewage sludge samples during pyrolysis. Kinetic parameters are determined by combining isoconversional and fitting methods. The integral methods of Flynn-Wall-Ozawa (FWO) and Kissinger-Akahira-Sunose (KAS) are used. The kinetic model is coupled with a stoichiometric reaction scheme to estimate the evolution of the solid, liquid and gas products. The suitability of the determined set of reaction parameters allows the simulation of the slow pyrolysis under different heating rates in the range between 100 K/min and 200 K/min and up to a high temperature of 960°C. This model offers a tool for the scale-up of the process as part of a project under development, aiming at the production and evaluation of pyrolysis chars from sewage sludge.

2. Materials and methods

2.1. Sewage sludge and products characterization

Anaerobically digested sewage sludge samples were obtained from the wastewater treatment plant El Salitre, located in Bogotá - Colombia. A total of 50 kg of dewatered sludge were pre-dried and crushed to obtain a homogeneous particle size (smaller than 3 mm). A sample of 1 kg was collected by quartering and submitted to a second drying step in a convection oven at 105°C during 10 h. After milling and sieving, particle sizes between 0.18 mm and 0.25 mm were obtained. The samples were afterward characterized as indicated in Table 2. Elemental analysis and low heating value (*LHV*) of the solid product were determined using the standards indicated in the table. The ash content of the solid product was determined from a mass balance using the ash content of the sewage sludge sample determined at 960°C. The *HHV* of the organic liquid was calculated from its elemental composition using the experimental correlation of (Li and Suzuki, 2010) presented in Eq. (1):

$$HHV_{Ol,d} = 34.09\,c_{Ol,d} + 132.2\,h_{Ol,d} + 11.99\,o_{Ol,d} \tag{1}$$

The low heating values (*LHV*) were calculated from the high heating values using an evaporation enthalpy of 2.44 MJ/kg. *LHV* of the gas product was obtained from its composition according to ISO 6976:2016.

Table 1. Kinetic parameters reported for pyrolysis of sewage sludge from urban water using a scheme of independent parallel reactions, under operational conditions similar to those used in this work. In all works, an Arrhenius expression is used for the velocity constant. For the concentration function of the kinetic expression, a power law is applied.

Country		US	Spain	Spain	Thailand	Spain	Poland	China
City		Princeton	Leon	Alicante	Bangkok	Sevilla	Katowice	Shenzhen
Heating rate/K/min		1 - 50	10	5 - 30	20	5 - 10	1 - 100	10
Final temperature /°C		600	650	550	600[1]	700	900	600
Decomposition of organic matter								
R1[6]	E_a/kJ/mol	130	205	103.9	91.9	79.07	-	39.1
	ln k_0/1/s	41.45	40.4	20.12	25.7	12.14	-	2.13
	n/1	10.0	2.4	4.13	1.03	0.96	-	1.94
	y/1	0.32	0.05	0.26	0.16	0.26	-	n.r.[2]
R2	E_a/kJ/mol	250.0	135.0	169.7	119.4	191.42	200.0	76.2
	ln k_0/1/s	57.56	21.99	28.98	29.7	33.59	37.35	11.33
	n/1	15.0	1.7	4.06	1.53	2.96	1.0	4.41
	y/1	0.68	0.49	0.57	0.15	0.32	0.41	n.r.
R3	E_a/kJ/mol	-	138.0	209.4	76.4	80.72	179.0	2.2e-14
	ln k_0/1/s	-	18.76	29.81	18.1	7.92	29.55	-7.85
	n/1	-	2.5	0.92	1.04	1.2	1.0	0.23
	y/1	-	0.44	0.18	0.18	0.28	0.09	n.r.
R4	E_a/kJ/mol	-	-	-	120.6	200.67	257.0	-
	ln k_0/1/s	-	-	-	22.8	20.48	39.92	-
	n/1	-	-	-	0.92	0.59	1.0	-
	y/1	-	-	-	0.41	0.1	0.22	-
Decomposition of inorganic matter								
R5	E_a/kJ/mol	-	-	-	-	101.14	237.0	-
	ln k_0/1/s	-	-	-	-	22.23	25.02	-
	n/1	-	-	-	-	2.95	1.0	-
	y/1	-	-	-	-	0.04	0.04	-
R6	E_a/kJ/mol	-	-	-	-	-	280.0	-
	ln k_0/1/s	-	-	-	-	-	26.58	-
	n/1	-	-	-	-	-	1.0	-
	y/1	-	-	-	-	-	0.06	-
Author		Urban and Antal	Calvo *et al.*	Font *et al.*	Thipkhunthod *et al.*	García *et al.*	Urych and Smolinski	Xu *et al.*
Year		1982[3]	2004	2005[3]	2007	2009[3]	2016[4,5]	2018

[1]Experimental work is performed until 800°C. Kinetic parameters are determined for reactions taking place until 600°C

[2]Not reported

[3]Mass fractions y_i are normalized to dry and ash-free basis

[4]Kinetic parameters calculated using the Kissinger isoconversional method of each reaction curve obtained by deconvolution of the experimental data

[5]The first reaction proposed in this work corresponds to the drying process of the sewage sludge sample. The parameters of this reaction are not reported here

[6]R1 to R6 correspond to each independent parallel reaction used for the kinetik analysis

2.2. Experimental facility and procedure

Experiments were carried out in a macro TGA equipped with a continuous evolved gas analysis system (EGA), as shown in Figure 1. In the following description the numbers refer to this figure. The cylindrical reactor is made of quartz glass and consists of a vertical cylinder and a sealing piece inserted at its top. The crucible hangs together with a quartz glass support from the balance (1). The sample temperature was measured with a K-type thermocouple placed inside the crucible, as shown in the detail of Figure 1. The reactor was externally heated by the electric furnace (2). Nitrogen 5.0 was used as carrier gas and fed at the top of the reactor through two mass flow controllers MFC1 and MFC2. The gas phase was evacuated at the bottom of the reactor and directed toward the tar condensers TC1 and TC2, where it was cooled down (between 0°C to 3°C) and separated from the condensed phase. Afterward, a fraction of the non-condensable gases passed through the continuous gas analysis system, composed of three analyzers for the measurement of H_2 and CH_4 (3), CO and CO_2 (4) and O_2 (5). O_2 was used as control value for the conservation of the inert atmosphere during the experiments. Then, the total gas flow was conducted to the gas meter (6). All measurements were recorded using the data acquisition module (7) and a computer.

Table 2: Fuel characterization, structural characterization and mineral matter composition of the sewage sludge used in this study, and data reported in the literature for comparison purposes. Standard deviations are calculated using three experimental replications.

Proximate analysis/wt%				
	Standard/Equipment (this study)	Colombia (this study)	Spain Calvo *et al.* (2004)	Turkey Karaca *et al.* (2018)
$M_{SS,ar}$	EN 14774-3	66.7 ± 0.5	n.r. [4]	n.r.
$M_{SS,ad}$	EN 14774-3	9.9 ± 0.2	7.9	6.0
$V_{SS,d}$	EN 15148	45.3 ± 0.5	42.9	55.5
$A_{SS,550,d}$	EN 14775	56.2 ± 0.2	53.8	35.5
$A_{SS,700,d}$	EN 14775[1]	53.7 ± 0,2	n.r.	n.r.
$A_{SS,800,d}$	EN 14775[1]	50.4 ± 0.2	n.r.	n.r.
$A_{SS,900,d}$	EN 14775[1]	47.2 ± 0.2	n.r.	n.r.
Elemental analysis/wt%				
$H_{HSS,d}$	EN15104	3.9 ± 0.2	3.3	4.3
$C_{HSS,d}$	EN15104	29.5 ± 0.4	22.7	34.1
$N_{HSS,d}$	EN15104	3.4 ± 0.2	3.1	5.3
$S_{HSS,d}$	ASTM D516	3.4 ± 0.2	0.9	1.0
$O_{HSS,d}$ [2]	-	12.6 ± 0.2	16.1	19.7
TOC[3]	AnalyticJena N/C3100	15.6 ± 0.4	n.r.	n.r.
LHV$_d$/MJ/kg	ASTM D240	11.3 ± 0.1	8.8	13.5
Structural composition/wt%, dry				
	Standard/Equipment (this study)	Colombia (this study)	China Wang *et al.* (2016)	USA Wesenbeeck *et al.* (2014)
Cellulose	van Soest *et al.*, 1991	4.5	n.r.	n.r.
Hemicellulose	van Soest *et al.*, 1991	5.7	n.r.	n.r.
Lignin	van Soest *et al.*, 1991	15.4	n.r.	n.r.
Heavy metals content/mg/kg$_{SS}$,dry				
As		450.0 ± 4.2	1983.8	67.6
Cd		< 1.0	1.7	3.6
Cu	Spectrometer Thermo	990.0 ± 5.3	3323.9	443
Hg	Electron Corporation S4	< 1.0	n.r.	0.27
Pb	AA-Serie	290.0 ± 2.7	69.7	41
Zn		4800.0 ± 21.3	2424.2	1360
Mineral composition/wt%, dry				
	Standard/Equipment (this study)	Colombia (this study)	China Tang *et al.* (2018)	USA Wesenbeeck *et al.* (2014)
SiO_2		22.3	5.4	13.4
Fe_2O_3		17.9	1.8	23.3
CaO		6.9	5.3	9.1
Al_2O_3	X Ray fluorescence	6.4	4.3	4.8
P_2O_5	spectrometer Philips ref.	6.1	6.6	21.3
TiO_2	MagicX PRO PW-2440	0.7	0.2	1.2
MgO		0.6	1.0	3.7
K_2O		0.6	1.1	2.4

[1]Modified according to the indicated final temperature
[2]Calculated by difference using the ash content determined at 960°C
[3]Total organic carbon
[4]n.r. Not reported

The experimental procedure started by weighting and placing the sample in the crucible, followed by assembling of the experimental setup. The flow of N_2 is fixed in MFC1 and MFC2 and the system was purged until measuring O_2 fractions lower than 0.05%. The heating program included a first drying stage where the sample was heated to 105°C until constant weight was obtained (40 min to 50 min). Afterwards, the temperature is increased using a constant heating rate until a final temperature of 960°C. This temperature was maintained during 30 min. The sample was then cooled down until room temperature under inert atmosphere. The char was removed from the reactor and weighed (with a precision of 0.1 mg).

2.3. Experimental plan

Experimental conditions to minimize heat and mass transfer effects and the occurrence of secondary reactions during pyrolysis were initially determined. A particle size between 0.18 mm and 0.25 mm, a bed height of 2 mm (corresponding to a dried sample of approx. 1 g) and

nitrogen flows of 0.3 l/min for MFC1 and 0.9 l/min for MFC2 (at environmental conditions) were used. Pyrolysis experiments using heating rates of 3 K/min, 5 K/min, 7 K/min, 10 K/min and 12 K/min until 960°C were carried out (at the heating rate of 10 K/min, experiments until 570°C are made in order to obtain solid samples for analysis). Reproducibility of experiments was determined by repetitions at 3 K/min and 10 K/min. Differences lower than 3.2% were obtained in the mass loss curves.
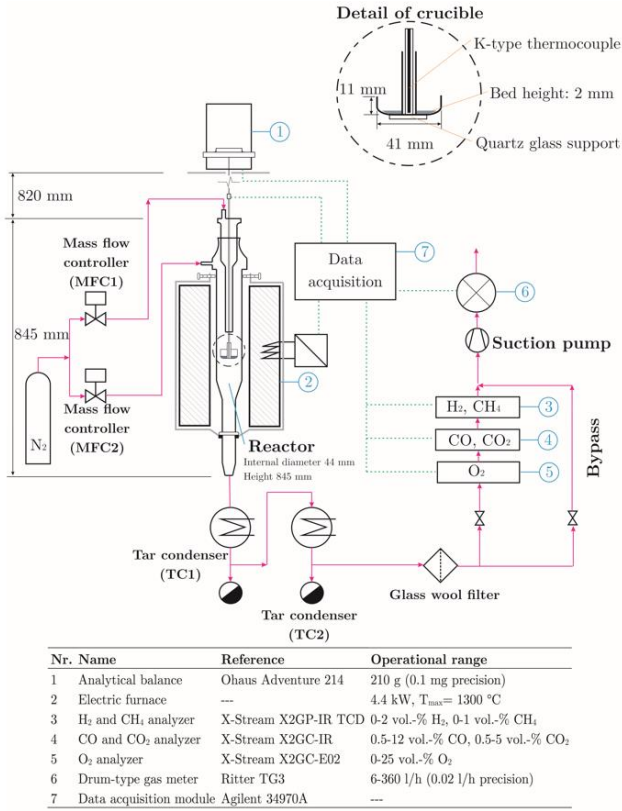

Figure 1 Experimental facility: Macro TGA equipped with evolved gas analysis (EGA).

2.4. Data analysis and calculations

Mass signal of the balance was corrected due to the force exerted on the crucible by the downward flow of nitrogen through blank measurements. Mass flows of CO, CO_2, CH_4 and H_2 were determined assuming ideal gas behavior of the gas mixture. The mass fraction of the liquid product (water + organic liquid) and its elemental composition were calculated by difference using the fractions of solid and gas products obtained at the temperature at which decomposition of organic matter is completed (established from the experimental results). The water content of the liquid product was determined using the approximation proposed by (Neves *et al.*, 2011). They stated that the mass fractions of C, H and N of the feedstock and those of the organic liquid (in ash-free and dry basis) are correlated in processing under conditions that avoid heat and mass transfer limitations. The values are slightly dependent on pyrolysis final temperature and for 570°C they ascend to 1.16 for $w_{C,SS,daf}/w_{C,Ol,daf}$; 0.8 for $w_{O,SS,daf}/w_{O,Ol,daf}$, and 1.14 for $w_{H,SS,daf}/w_{H,Ol,daf}$. The water content was calculated as the amount that minimizes the

difference of these values and those obtained using the experimental data.

Normalized mass loss of the sewage sludge ($w_{SS,d}$) was calculated using the corrected mass signal of the balance ($m_{S,d}$) and the initial mass of the sewage sludge in dry basis ($m_{SS,0,d}$). Mass yields ($y_{M,p}$) of pyrolysis products were calculated from the mass of each product ($m_{p,d}$), according to Eq. (2):

$$y = \frac{m_{p,d}}{m_{SS,0,d}} \qquad (2)$$

Energy balances were determined at 25°C using the low heating value of each material.

2.5. Kinetic model

A formal independent parallel reactions model was implemented for the description of the pyrolysis kinetics of sewage sludge. The reaction rate with N number of pseudo-components can be expressed as in Eq. (3):

$$\frac{dw_{RM}}{dt} = -\sum_{i=1}^{N} y_i k_{0,i} \exp\left(\frac{-E_{a,i}}{RT}\right) w_{RM}^{n_i} \qquad (3)$$

where w_{RM} represents the normalized fraction of the reacting mass of each component. The parameters (N, y_i, $E_{a,i}$, $k_{0,i}$ and n_i) were determined by applying a combination of isoconversional methods and a model-parameter fitting method, as follows. First, experimental values of w_{RM} were determined using Eq. (4),

$$w_{RM} = \frac{m_{RM}}{m_{RM,0}} = \frac{m_{S,daf} - m_{char,f,daf}}{m_{SS,0,daf} - m_{char,f,daf}}. \qquad (4)$$

The experimental mass measured by the balance (m_S) at each point in time corresponds to the sum of the reacting mass (m_{RM}) and the mass of the produced solid or char (m_{char}). In order to obtain the value of reacting mass, it was assumed that the fraction of char corresponds in all times to the relation $m_{char,f}/m_{SS,0}$. Mass values in ash-free basis were calculated using the ash content measured at 960°C. An initial set of indicative values of activation energies for the pyrolysis of the pseudo-components was determined using the isoconversional methods of FWO and KAS. Their corresponding linear expressions are presented in Eq. (5) and Eq. (6), respectively (Flynn, 1997):

$$(\ln \kappa) = \text{Const} - 1.052 \left(\frac{E_a}{RT}\right)_{w_{RM}} \qquad (5)$$

$$\left(\ln \frac{\kappa}{T^2}\right) = \text{Const} - \left(\frac{E_a}{RT}\right)_{w_{RM}}. \qquad (6)$$

The methods were evaluated for w_{RM} values ranging from 95 wt% to 5 wt% using steps of 5 wt%. The obtained values for the activation energies were used afterward in the model fitting-step as target values. An initial number of pseudo-components was established from the number of discernible peaks obtained in the experimental curves of mass loss rate (dw_{RM}/dt). Based on Eq. 3, a first set of kinetic parameters $E_{a,i}$ and $k_{0,i}$ for each reaction was determined from an Arrhenius diagram

$\left(\ln\left(\dfrac{dw_{RM}/dt}{w_{RM}^{n}}\right) vs. 1/T\right)$ by linear regression in the time interval in which the analyzed reaction takes place. The reaction order was initially set to $n_i = 1$ for each reaction. The fraction y_i was calculated as the relationship between the peak heights of the theoretical and the experimental curves. The parameters of the last reaction were first determined and then the calculated mass loss and mass loss rates were subtracted from the experimental values. The parameters of the additional reactions were successively determined using the same procedure. In this way, influences caused by parallel reactions occurring in the same temperature interval are minimized. After determining the first set of initial parameters values, a minimization procedure was performed. The peak position and area of the corresponding reaction were varied simultaneously to obtain a minimum error between the experimental and the calculated differential mass curves by varying $E_{a,i}$, $k_{0,i}$ and n_i. The quality of the minimization was evaluated by the least squares method, calculating the residual sum of squares (RSS) and the fit of the experimental and calculated curves using Eq. (7) and (8), respectively (where z corresponds to the number of data acquired during experimentation):
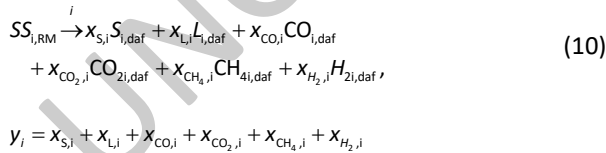
$$RSS = \sum_{1}^{z}\left((dw_{RM}/dt)_{exp} - (dw_{RM}/dt)_{cal}\right)^2 ; \qquad (7)$$

$$Fit = \sqrt{\frac{RSS}{z}}. \qquad (8)$$

The mass of products obtained during sewage sludge pyrolysis was determined using Eq. (9) as the sum of the contributions of the products of the decomposition of each pseudo-component:

$$y_{M,p} = \sum_{i=1}^{N} y_{M,p,i}. \qquad (9)$$

Product evolution of each pseudo-component was estimated using the global stoichiometric model presented in Eq. (10) and the condition of Eq. (11):

$$SS_{i,RM} \xrightarrow{i} x_{S,i} S_{i,daf} + x_{L,i} L_{i,daf} + x_{CO,i} CO_{i,daf} + x_{CO_2,i} CO_{2i,daf} + x_{CH_4,i} CH_{4i,daf} + x_{H_2,i} H_{2i,daf}, \qquad (10)$$

$$y_i = x_{S,i} + x_{L,i} + x_{CO,i} + x_{CO_2,i} + x_{CH_4,i} + x_{H_2,i}$$

The stoichiometric coefficients $x_{S,i}, x_{L,i}, x_{CO,i}, x_{CO_2,i}, x_{CH_4,i}, x_{H_2,i}$ were calculated by minimizing the difference between the experimental evolution of each species and the simulated mass flow rates. The coefficient $x_{L,i}$ for the liquid product was calculated by difference.

3. Results and discussion

3.1. Thermal decomposition of sewage sludge

Figure 2(a) shows the mass loss and the mass loss rate (as $dw_{SS,d}/dT$) of the sewage sludge thermal decomposition until 960°C for heating rates between 3 K/min and 12 K/min. The evolved mass curves of gaseous products and their mass production rate at 10 K/min are presented in Figure 2(b) and (c). Thermal decomposition can be divided in two zones: A low temperature zone (Zone I) from 120°C until a temperature between 550°C and 590°C and a high temperature zone (Zone II), for temperatures between the end of zone I until 960°C. Zone I can be mainly attributed to decomposition of organic matter. Temperatures in the range between 500°C and 550°C have been reported as the final values for thermal degradation of lignocellulosic biomass, lipids and proteins (Arenas *et al.*, 2019; Cortés and Bridgwater, 2015; Zhu, 2019). In zone II, mainly the decomposition of inorganic matter and secondary decomposition reactions of primary char and tar take place (Antal *et al.*, 1998; Casajus *et al.*, 2009; Karayildirim *et al.*, 2006; Thipkhunthod *et al.*, 2007). The influence of the heating rate variation on the process is small in the range studied in this work, being more pronounced in the low temperature zone. With increasing heating rate, a reaction shift to higher temperatures in the whole temperature range is observed. This behavior has been attributed to a shorter exposure time to temperature, causing that the decomposition partially occurs at higher temperatures (Antal *et al.*, 1998). An increasing difference between the measured and the true sample temperatures (thermal lag) have been also detected when the heating rate increases. Consequently, the temperature at which the transition between zone I and zone II takes place slightly increases with an increase in the heating rate. At 3 K/min, the measured transition takes place at 550°C, while at 12 K/min, it occurs at 585°C. Other works on pyrolysis of sewage sludge in TGA report values between 500°C and 677°C (Casajus *et al.*, 2009; García *et al.*, 2009; Urych and Smolinski, 2016; Zhu *et al.*, 2019) for this transition.

The following paragraphs present a description of the course of the thermal decomposition based on the results at 10 K/min. In zone I, the mass loss rate curve shows a shoulder at temperatures lower than 240°C and two distinguishable peaks at 340°C and 430°C. Thermal degradation below 250°C is typically attributed to organic compounds with low stability, non-biological substances, dead bacteria and simple lipids and aminoacids, among others (Calvo *et al.*, 2004; Font *et al.*, 2005; Thipkhunthod *et al.*, 2007, Urban and Antal, 1982; Urych and Smolinski 2016). Thermal decomposition of these compounds is included in the first decomposition reaction of organic matter in the kinetic studies shown in Table 1. Hemicellulose, whose decomposition starts at temperatures as low as 200°C (Yang *et al.*, 2007; Zhu *et al.*, 2019), is included either in the first reaction or as a single compound in reaction R2 (Calvo *et al.*, 2004; García *et al.*, 2009). Font *et al.*, 2005 attributed the first reaction to hemicellulose and the second reaction to dead bacteria. The second global reaction of decomposition occurs approximately between 220°C and 400°C, as shown in Figure 2(a). In addition to hemicellulose, at these temperatures, cellulose, lignin and proteins decomposition takes place (Yang *et al.*, 2007; Varhegy *et al.*, 2007; Thipkhunthod *et al.*, 2007). Above 400°C,

decomposition is caused mainly by lignin (Yang *et al.*, 2007) and lipids (Thipkhunthod *et al.*, 2007, Zhu *et al.*, 2019). Xu *et al.*, 2018 attributed reaction R3 to aromatic compounds and polyphenols. Mass loss in zone I can also be affected by decomposition of other organic compounds present in smaller quantities, such as starch, humic acids, nucleic acids, coagulants, plastics and fractions of waste tires (Thipkhunthod *et al.*, 2007; Wang *et al.*, 2019), and to decomposition of inorganic compounds with low decomposition temperatures.

Regarding gas evolution, the predominant gas species is CO_2, followed by CO (Figure 2(b)). CH_4 and H_2 account for a small fraction of the total gas production (Figure 2(c)). The mass production rates of CO_2 and CO show a peak, each with maximum rates at 405°C and 420°C, respectively. The formation of these peaks can be attributed mainly to protein and lignin decomposition, as CO_2 and CO production from hemicellulose and cellulose occurs at lower temperatures, and production of lipids at higher ones. Moreover, lime (CaO), which is added during sewage treatment and is present in a considerable amount in the ash of the analyzed sample (see Table 2), can absorb CO_2 evolved in this zone (Chanaka *et al.*, 2019b). CH_4 formation is mainly associated with primary pyrolysis reactions of lignin and with decomposition of proteins (due to dead bacteria) at temperatures below 500°C (Gao *et al.*, 2014; Yang *et al.*, 2007). H_2 evolution shows the typical course observed during pyrolysis of lignocellulosic biomass.

In zone II, from 570°C onward, a continuous increment in the mass loss rate is detected (Figure 2 (a)). This increment takes place simultaneously with an increase in the gas evolution caused mainly by CO and CO_2, as presented in Figure 2 (b) and (c). Decomposition of inorganic matter in zone II is included in the models of (García *et al.*, 2009; Urych and Smolinski 2016) (Table 1), but no reference to the involved compounds is made. As shown in Table 2, iron and silicon are found in larger amounts in the sample, followed by calcium, aluminum and phosphorus. CO_2 evolution between 600°C and 800°C can be associated with decomposition of calcium carbonate $CaCO_3$ to CaO (Karayildirim *et al.*, 2006). Part of this CO_2 could have been originated and adsorbed by CaO in zone I. The release of CO between 570°C and 960°C, observed in Figure 2(b), can be attributed to three pathways: First, the reaction of Fe_3O_4 with C to Fe and CO (Furimsky and Sears, 1988). Second, char gasification inside the char particles according to the Boudouard reaction favoring the formation of CO at the expense of CO_2. Third, thermal cracking of hydrocarbons filling the porous structure of the solid phase. This reaction causes at the same time the decrease of CH_4 and the steep increase in H_2 observed at temperatures higher than 650°C (Chanaka *et al.*, 2019a; Morf, 2002). Pathways 2 and 3 are catalyzed in the presence of CaO (Chanaka *et al.*, 2019a). Additionally, dehydrogenation reactions that occur at temperatures above 450°C Porada, 1959 can also contribute to H_2 formation. Silicon and aluminum are present as oxides or as silicates and aluminosilicates of

metals (for the analyzed sample, mainly of Ca and Fe and in a minor proportion of Mg and K). These compounds undergo solid state transformations at high temperatures without the release of gaseous species or are stable in the temperature range studied (i.e. SiO_2 and Al_2O_3) (Roedder, 1959). A small influence on CO_2 formation may arise from the reaction of silicon oxide with potassium carbonate to form potassium silicates (Roedder, 1959). Although the influence of silicates and aluminosilicates in the pyrolysis process has not been deeply studied, they play an important role in heavy metal immobilization in the solid product by the formation of thermally stable, acid insoluble compounds (Chanaka *et al.*, 2019a, 2019b).
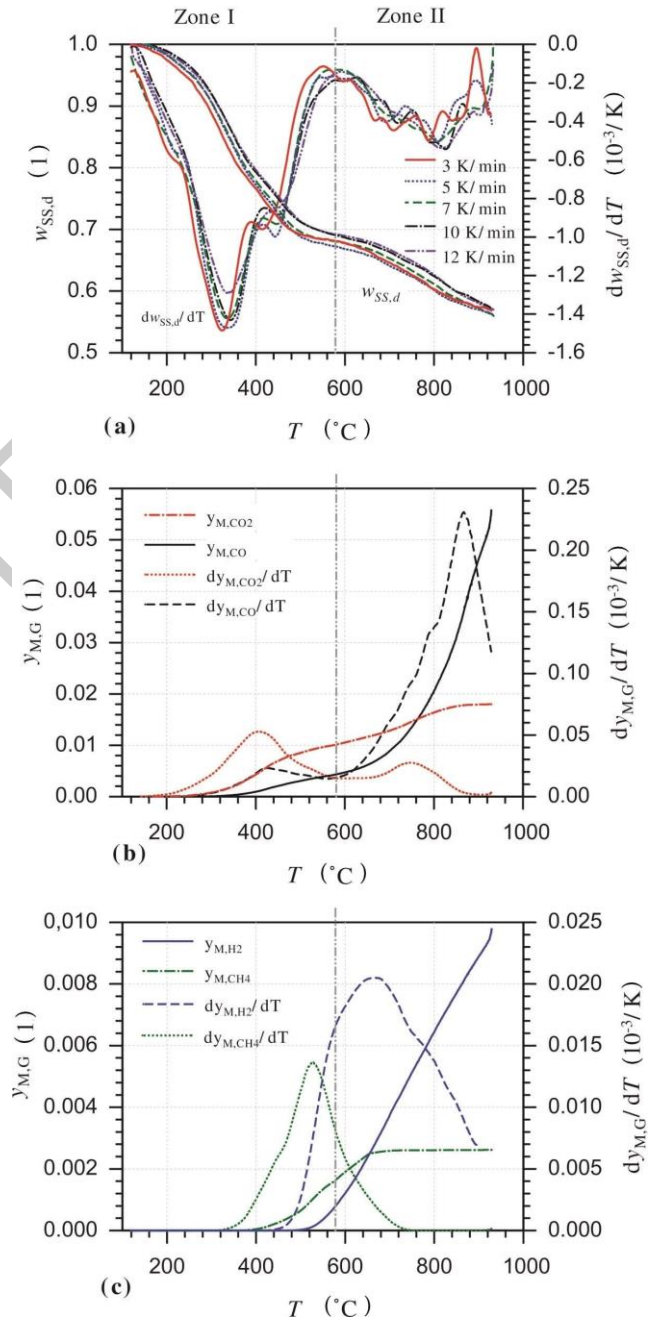

Figure 2 Mass loss and mass loss rate at different heating rates (a), mass production rate and mass production of CO and CO_2 (b), and mass production rate and mass production of H_2 and CH_4 (c) during sewage sludge pyrolysis at 10 K/min until a final temperature of 960°C.

3.2. Mass and energy balances

Figure 3 shows Sankey diagrams for the mass and energy balances for the pyrolysis of sewage sludge at 10 K/min until 570°C and between 570°C and 960°C. Errors in mass and energy balances are presented as differences in these diagrams. Detailed results of mass and elements balances are included in Tables 4 and 5 in the Appendix A. Mass loss of sewage sludge in dry basis during pyrolysis until 960°C amounts to 43.1 wt%. A fraction of 71.4 wt% of this decomposition (30.8 wt% of the dry sewage sludge mass) takes place in zone I and the rest occurs in zone II. The obtained solid fraction is in the range of the highest values found in the literature, while the gaseous fraction is around the lowest (Álvarez *et al.*, 2015; Trinh *et al.*, 2013). The liquid fraction is between the average of the reported values (Álvarez *et al.*, 2015; Sánchez *et al.*, 2009). Its calculated water content according to section 2.4 amounts to 18.2 wt%. Reported values of water content for this fraction vary between 10 wt% and 65 wt% (in dry basis) (Rincón *et al.*, 2019; Sánchez *et al.*, 2009; Trinh *et al.*, 2013; Urych and Smolinski, 2016). The extent to which thermal decomposition of inorganic matter in zone II takes place is approximately determined as follows: $Solid_1$ losses 17.8 wt% of its mass in this zone. Under the supposition that the same amount of mineral matter decomposes at combustion and at pyrolysis conditions, the difference between the ash content measured at 550°C and that at 960°C (see Table 2) equals the volatilized mineral matter in this zone. Its value amounts to 9 wt% of the initial sewage sludge mass or 13 wt% of $Solid_1$ and corresponds to 73 wt% (13 wt%/17.8 wt%) of the mass loss of $Solid_1$. The remaining 27 wt% of this mass loss is then caused by secondary reactions of the residual organic matter. Ash contents of 68.2 wt% and of 82.9 wt% are calculated for $Solid_1$ and $Solid_2$, respectively. Total mineral matter of $Solid_1$, determined as the sum of volatile mineral matter and ash, amounts to 81.2 wt%. In terms of the element balances, the mass of carbon after pyrolysis up to 570°C is approximately evenly distributed in the solid and liquid products. 73 wt% of the mass of hydrogen and 70 wt% of the mass of oxygen originally present in the dried sewage sludge are in the liquid product after pyrolysis. After subsequent heating to 960°C, 25 wt% of the mass of carbon present in the sewage sludge remains in the solid product, while hydrogen and oxygen pass almost completely into the gaseous phase.

The *LHV* in dry basis of each material presented in Figure 3(b) are 7.77 MJ/kg for $Solid_1$, 5.19 MJ/kg for $Solid_2$, 12.16 MJ/kg for Gas_1, 24.29 MJ/kg for Gas_2 and 33.42 MJ/kg for organic liquid. From the energy balance, a value of 2.18 MJ/kg of dry sewage sludge, or 19.4% of its *LHV*, is calculated for the energy required for the pyrolysis until 570°C. The liquid product (organic liquid plus pyrolysis water) has the highest energy fraction followed by the solid product. The former amounts to 58.5% and the latter to 40.0% of the energy entering the process. The energy fraction of the gas product at 570°C is negligible. The energy content of the evolved gases in the high temperature zone equals 13.4% of the energy contained

in the dry sewage sludge. The difference in the energy balance originates from the error in the mass balance. As decomposition reactions of inorganic compounds of Ca and Fe as well as secondary cracking and gasification reactions are mostly endothermic, an overall endothermic reaction of the process is expected in the high temperature zone.
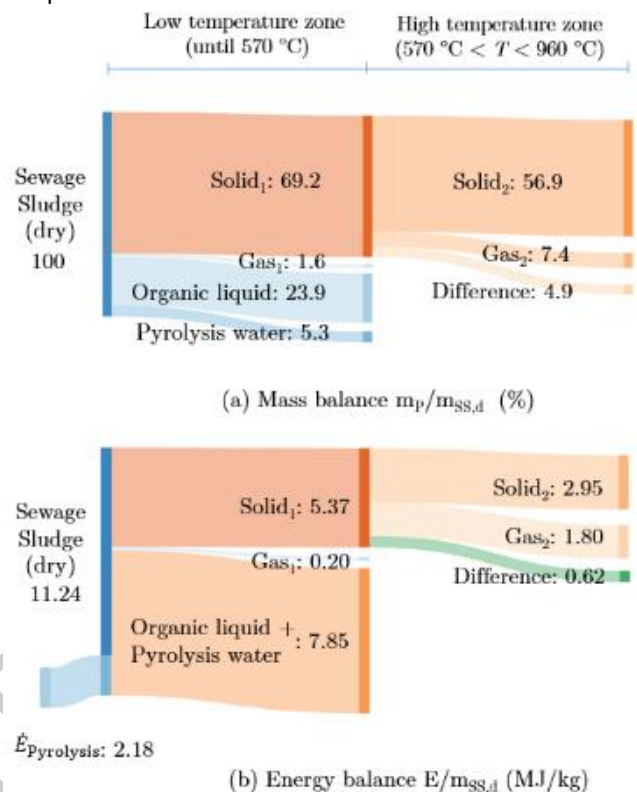

(a) Mass balance $m_P/m_{SS,d}$ (%)

(b) Energy balance $E/m_{SS,d}$ (MJ/kg)

Figure 3 Mass and energy balances for the pyrolysis of sewage sludge at 10 K/min until 570°C and 960°C.
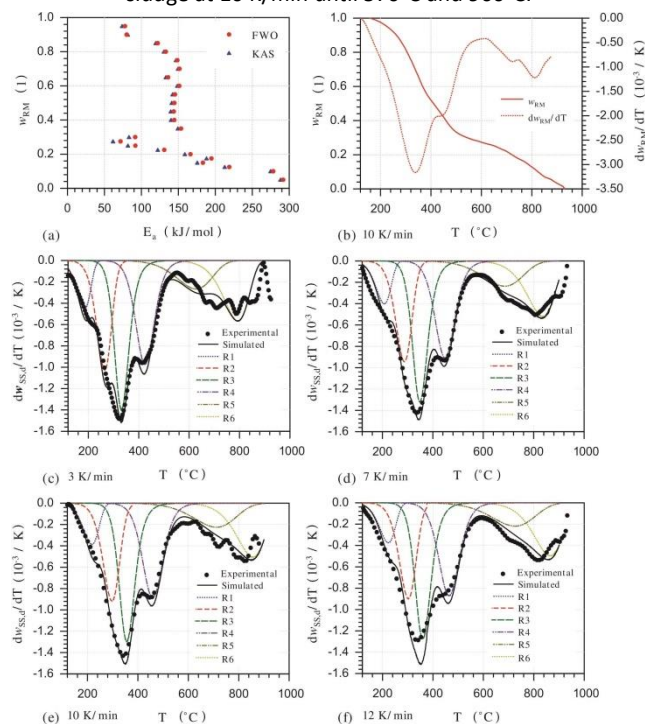

Figure 4 Activation energy values for conversion steps of 5 wt-% by the FWO and KAS isoconversional methods (a), mass loss (w_{RM}) and mass loss rate (as dw_{RM}/dT) at 10 K/min (b), and experimental and simulated mass loss rate curves of sewage sludge pyrolysis at different heating rates (c to f).

The low influence of heating rate on product yield, observed in Table 4, is attributed to the high content of mineral matter of the sewage sludge used in this work which exerts a pronounced catalytic effect on the pyrolysis reactions.

3.3. Implementation of the kinetic model

Figure 4(a) shows the variation of E_a with w_{RM} obtained from the application of the isoconversional methods of FWO and KAS, according to Eq. (5) and Eq. (6). Experimental values of w_{RM} and dw_{RM}/dT for 10 K/min are shown in Figure 4(b). Arrhenius plots and the values of E_a, along with the correlation coefficient of each linear fitting, are included in Figure 6 and Table 6 of the Appendix A. Maximal variations in E_a, between both methods are around 5% in zone I and 14% in zone II, therefore, any of them can be used to obtain the first estimated values of the activation energy for the pyrolysis process at different conversion levels. The variations in E_a with w_{RM} in the range between 95 wt% and 70 wt% (up to about 350°C) and from 25 wt% until the end of the process (above 600°C) indicate that the overall decomposition is the result of the decomposition of several individual components. On the other hand, narrow variations around a value of E_a = 150 kJ/mol for w_{RM} between 70 wt% and 35 wt% (between 350°C to 500°C) indicate that the process is dominated in this range by a single compound or that it takes place over several compounds with similar E_a. In the transition region between zone I and zone II, the strong decrease in the values of E_a is caused by the completion of the decomposition reactions of the organic matter.

A set of four reactions in zone I and two reactions in zone II appropriately fit the sewage sludge thermal decomposition of the samples used in this study. Table 3 presents the calculated kinetic parameters and the stoichiometric coefficients for the estimation of the simulated curves of mass loss, mass loss rate and product evolution. Figure 4(c) to Figure 4(f) show the comparison

of simulated results of $dw_{SS,d}/dT$ with experimental data for different heating rates. The calculated curves adequately reproduce the experimental mass loss for the heating rates used. The maximal deviation calculated according to Eq. (8) equals 9.0%, mainly due to differences in the peak heights of zone I, which are accentuated by increasing heating rates. According to the analysis presented in section 3, reactions R1 and R2 relate to the degradation of extractives and a fraction of hemicellulose. Reactions R3 and R4 are responsible for the decomposition of cellulose, lignin, proteins, lipids and some plastics. Reactions R5 and R6 represent the decomposition of volatile inorganic matter and secondary decomposition of residual organic matter. From the studies presented in Table 1 Font *et al.*, 2005 reported a similar variation of E_a with conversion to that found in the present study.
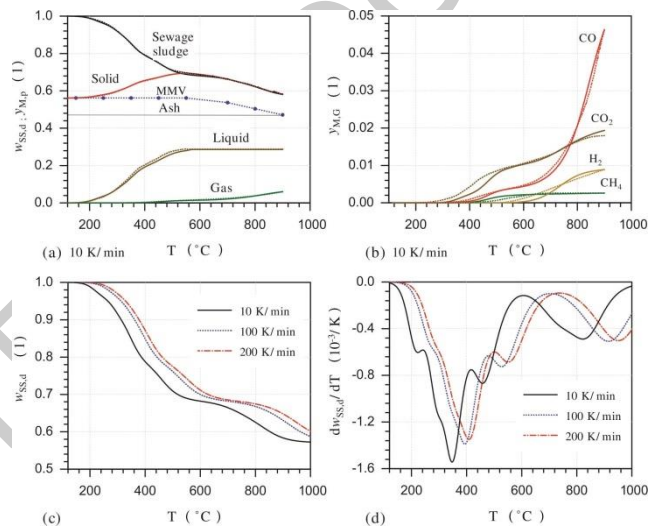

Figure 5 Mass loss and product evolution during the pyrolysis of sewage sludge at 10 K/min (a and b), and simulated curves of mass loss and mass loss rates (as $dw_{SS,d}/dT$) (c and d) during sewage sludge pyrolysis at 10 K/min, 100 K/min and 200 K/min.

Table 3: Kinetic parameters determined in this study for the independent parallel reactions model of the sewage sludge pyrolysis, and stoichiometric coefficients of products (char (S), liquid (L), CO, CO_2, CH_4 and H_2) for each independent parallel reactions according to Eq. (10)

Reactions	R1	R2	R3	R4	R5	R6
Kinetic parameters for the independent parallel reactions						
$E_{a,i}$/kJ/mol	90.36	128.00	150.57	147.82	151.46	250.51
ln $k_{0,i}$/1/s	17.20	22.42	24.07	18.80	12.23	21.50
y_i/1	0.10	0.13	0.29	0.22	0.12	0.14
n_i/1	2.00	1.80	2.40	2.20	1.50	2.00
Stoichiometric coefficients of products						
$x_{S,i}$	0.033	0.042	0.095	0.062	0.044	0.047
$x_{L,i}$	0.067	0.087	0.192	0.138	0.000	0.000
$x_{CO,i}$	0.000	0.001	0.001	0.007	0.011	0.041
$x_{CO2,i}$	0.000	0.000	0.003	0.011	0.007	0.002
$x_{CH4,i}$	0.000	0.000	0.000	0.003	0.000	0.000
$x_{H2,i}$	0.000	0.000	0.000	0.000	0.008	0.000

As presented in Figure 5 (a and b), simulated and experimental curves of mass loss and evolution of products show good agreement. The change in ash

content above 570°C is included in the mass loss curve. Figure 5 (c and d) show the simulated mass loss and mass loss rate curves (as $dw_{SS,d}/dT$) for the pyrolysis of the

sewage sludge sample analyzed in this study, using higher heating rates of 100 K/min and 200 K/min (and those for 10 K/min for comparison purposes). Since no considerable changes in solid yield with the heating rate are expected, the value obtained at 960°C is used for the solid yield needed for the implementation of the model. Even with higher heating rates than those used to determine the set of kinetic parameters, an adequate reproduction of the mass loss curves and their peaks during pyrolysis is obtained. In their experiments in TGA at 100 K/min, Urych and Smolinski, 2016 measured a transition temperature between zone I and zone II of 700°C, corresponding to an increment in 75°C with respect to the value obtained at 10 K/min. This test indicates the suitability of the kinetic parameters determined for use at higher heating rates, but their validation requires additional experimental work.

4. Conclusions

The pyrolysis of sewage sludge allows the generation of valuable products that can be used as energy source or as raw material for further applications. In the temperature range from 550°C to 600°C, the thermal degradation of most of the organic material is completed. From this temperature and up to high pyrolysis temperatures of 960°C, further reactions of the solid residue occur. These reactions correspond to volatilization of Fe- and Ca-compounds and to secondary reactions of remaining organic matter. The product yields are strongly influenced by the final temperature, while the influence of the heating rate is negligible. The yield of the solid residue depends especially on the content of inorganic material. Gas production until 570°C amount to just 1.6 wt% of the initial dry sewage sludge sample, while liquid production amount to 29.2 wt% and char to 69.2 wt%. An increment in the final temperature to 960°C leads to an increase in the gas production to 7.4 wt% and a reduction in the solid yield to 56.9 wt%.

A reaction enthalpy of 19.4% of the lower calorific value of the dry sewage sludge is determined for pyrolysis up to 570°C. Until this temperature the energy entering the process is distributed into fractions of 58.5%, 40.0% and 1.5% for liquid, solid and gaseous products, respectively. Further increase of the pyrolysis temperature up to 960°C

causes a decrease in the energy fraction of the solid residue to 22.0%. The energy fraction of the gaseous product generated in this temperature region amounts to 13.4% of the energy entering the process.

The use of fitting and isoconversional methods coupled in a formal semi-global reaction scheme for pyrolysis allows establishing a set of reaction kinetic parameters suitable for the simulation of the process, which presents an appropriate stability even for heating rates up to 200 K/min. These results are an important tool for the development and scale-up of the pyrolysis process of sewage sludge in reactors operating at heating rates of this order of magnitude.
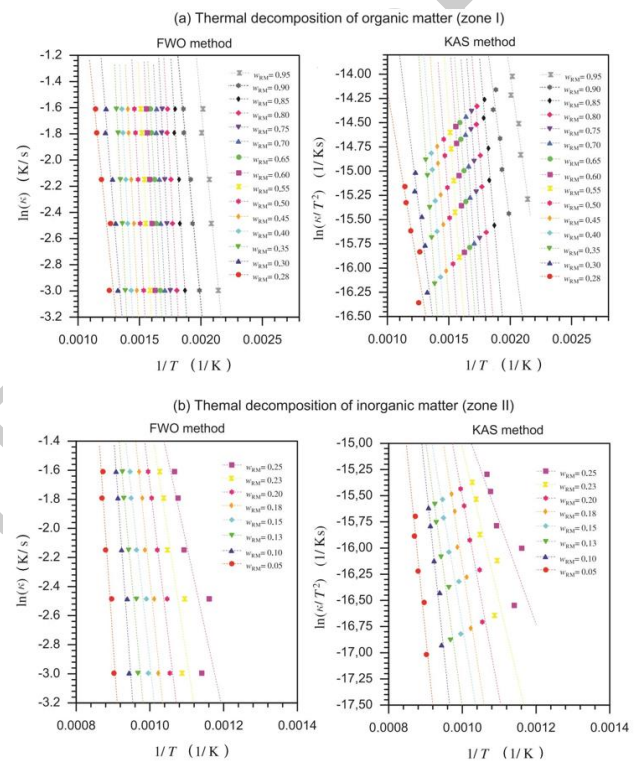
Appendix A

Figure 6: Arrhenius plots for the determination of E_a using the FWO and KAS isoconversional methods.

Table 4: Mass balances for the pyrolysis of sewage sludge at different heating rates until the transition temperature between zone I and zone II and until 960°C. The mass of the liquid product at 960°C is the same as that at the transition temperature since it is assumed that no further changes at high temperatures take place in this phase. All values are in dry basis (S, solid; L, liquid)

	Temperature	Product yields/1						
		$y_{S,d}$	$y_{L,d}$	$y_{CO,d}$	$y_{CO2,d}$	$y_{CH4,d}$	$y_{H2,d}$	Total
TG1 (3 K/min)	560°C	0.6878	0.2984	0.0056	0.0057	0.0010	0.0015	1.0000
	960°C	0.5685	0.2984	0.0637	0.0092	0.0010	0.0094	0.9530
	$\Delta y_{p,960\text{-}560°C}$	-0.1194	0.0000	0.0582	0.0034	0.0000	0.0079	-0.0498
TG2 (7 K/min)	565°C	0.6822	0.2941	0.0076	0.0117	0.0027	0.0016	1.0000
	960°C	0.5610	0.2941	0.0692	0.0152	0.0030	0.0085	0.9511
	$\Delta y_{p,960\text{-}565°C}$	-0.1212	0.0000	0.0616	0.0035	0.0003	0.0068	-0.0489
TG3 (10 K/min)	570°C	0.6919	0.2917	0.0041	0.0100	0.0016	0.0007	1.0000
	960°C	0.5687	0.2917	0.0588	0.0183	0.0026	0.0106	0.9507
	$\Delta y_{p,960\text{-}570°C}$	-0.1232	0.0000	0.0547	0.0083	0.0010	0.0099	-0.0493

TG4 (12 K/min)	585°C	0.6865	0.2939	0.0051	0.0117	0.0022	0.0006	1.0000
	960°C	0.5706	0.2939	0.0522	0.0179	0.0027	0.0099	0.9472
	$\Delta y_{p,960-585°C}$	-0.1159	0.0000	0.0471	0.0062	0.0005	0.0093	-0.0528

Table 5: Element balances for the pyrolysis of sewage sludge at 10 K/min until 570°C and 960°C. Elemental analysis of the liquid product at 960°C is the same as that at 570°C since its formation is completed at 570°C

	Final temperature 570°C							
	Sewage sludge				**Products**			
		Solid	Liquid	CO	CO$_2$	CH$_4$	H$_2$	Total
		Element composition based on the dry mass of each product $m_{element}/m_p$						
C	0.2947	0.2069	0.5000	0.4288	0.2729	0.7487	-	
H	0.0391	0.0134	0.0987	-	-	0.2513	1.000	
O	0.1262	0.0420	0.3001	0.5712	0.7271	-	-	
N	0.0343	0.0213	0.0670	-	-	-	-	
S	0.0338	0.0344	0.0343	-	-	-	-	
		Element composition based on the dry mass of sewage sludge $m_{element}/m_{SS,d}$						
y_C		0.1432	0.1459	0.0018	0.0027	0.0012	-	0.2947
y_H		0.0093	0.0288	-	-	0.0004	0.0007	0.0391
y_O		0.0290	0.0875	0.0024	0.0073	-	-	0.1262
y_N		0.0147	0.0196	-	-	-	-	0.0343
y_S		0.0238	0.0100	-	-	-	-	0.0338
	Final temperature 960°C							
	Sewage sludge	Products						
		Solid	**Liquid**	CO	CO$_2$	CH$_4$	H$_2$	Total
		Element composition based on the dry mass of each product $m_{element}/m_p$						
C	0.2947	0.1296	0.5000	0.4288	0.2729	0.7487	-	
H	0.0391	0.0028	0.0987	-	-	0.2513	1.000	
O	0.1262	0.0115	0.3001	0.5712	0.7271	-	-	
N	0.0343	0.0042	0.0670	-	-	-	-	
S	0.0338	0.0221	0.0343	-	-	-	-	
		Element composition based on the dry mass of sewage sludge $m_{element}/m_{SS,d}$						
y_C		0.0737	0.1459	0.0252	0.0050	0.0019	-	0.2517
y_H		0.0016	0.0288	-	-	0.0007	0.0106	0.0416
y_O		0.0065	0.0875	0.0336	0.0133	-	-	0.1410
y_N		0.0024	0.0196	-	-	-	-	0.0220
y_S		0.0126	0.0100	-	-	-	-	0.0226

Table 6: Calculated activation energies and correlation coefficient of the linear fitting as a function of w_{RM}

	FWO method		**KAS method**	
w_{RM}	E_a/kJ/mol	r^2	E_a/kJ/mol	r^2
	Thermal decomposition of organic matter (zone I)			
0.95	77.9	0.95	73.9	0.94
0.90	80.0	0.98	81.5	0.90
0.85	122.11	0.94	119.4	0.94
0.80	133.0	0.97	130.4	0.96
0.75	148.7	0.97	146.7	0.97
0.70	151.6	0.97	149.5	0.98
0.65	136.1	0.99	133.0	0.99
0.60	151.6	0.99	148.6	0.99
0.55	145.4	0.99	142.3	0.99
0.50	144.6	0.99	141.0	0.99
0.45	143.8	0.99	139.8	0.99
0.40	144.5	0.99	140.0	0.99
0.35	153.6	0.99	149.3	0.99
0.30	91.6	0.91	83.3	0.89
0.28	71.7	0.85	61.6	0.79
	Thermal decomposition of inorganic matter (zone II)			
0.25	91.9	0.75	81.7	0.68
0.23	131.0	0.82	122.1	0.78
0.20	166.3	0.95	158.8	0.94

0.18	194.7	0.96	188.1	0.95
0.15	183.2	0.93	175.6	0.91
0.13	218.9	0.93	212.7	0.92
0.10	278.2	0.96	274.7	0.95
0.05	291.7	0.93	288.1	0.92

Nomenclature

Symbol

A	Ash content, wt%
k_0	Pre-exponential factor, 1/s
E	Energy, MJ
E_a	Activation energy, kJ/mol
M	Moisture, wt%
m	Mass, g
n	Reaction order
T	Temperature, °C
t	Time, s
V	Volatile matter, wt%
w	Mass fraction, wt%
x	Stoichiometric coefficient, wt%
y_M	Mass yield
κ	Heating rate, K/min

Subscript

ad	As determined
ar	As received
cal	Calculated
d	Dry basis
daf	Dry and ash free basis
exp	Experimental
f	Final
G	Gas
i	Pseudo-component
inorg	Inorganic
L	Liquid
Ol	Organic liquid
Org	Organic
p	Product
RM	Reacting mass
S	Solid
SS	Sewage sludge
t	Theoretical
0	Initial

References

Álvarez J., Amutio M., López G., Barbarias I., Bilbao J. and Olazar M. (2015). Sewage sludge valorization by ash pyrolysis in a conical spouted bed reactor. *Chemical Engineering Journal*, **273**, 173–183.

Anca-Couce A., Berger A. and Zobel N. (2014). How to determine consistent biomass pyrolysis kinetics in a parallel reaction scheme. *Fuel*, **123**, 230–240.

Antal M., Varhegyi G. and Jakab E. (1998). Cellulose pyrolysis kinetics: Revisited. *Industrial & Engineering Chemistry Research*, **37**, 1267–1275.

Arenas C., Navarro M. and Martínez J. (2019). Pyrolysis kinetics of biomass wastes using isoconversional methods and the distributed activation energy model. *Bioresource Technology*, **288**, 121485.

Bergfeldt B., Morgano M.T., Leibold H., Richter F. and Stapf D. (2018). Recovery of phosphorous and other nutrients during pyrolysis of chicken manure, *Agriculture*, **8**, 1–10.

Calvo L., Otero M., Jenkins B., García A.I. and Morán A. (2004). Heating process characteristics and kinetics of sewage sludge in different atmospheres. *Thermochimica Acta*, **409**, 127–135.

Casajus C., Abrego J., Marias F., Vaxelaire J., Sánchez J. and Gonzalo A. (2009). Product distribution and kinetic scheme for the fixed bed thermal decomposition of sewage sludge. *Chemical Engineering Journal*, **145**, 412–419.

Chanaka W., Veksha A., Giannis A. and Lim T.-T. (2019a). Pyrolysis derived char from municipal and industrial sludge: Impact of organic decomposition and inorganic accumulation on the fuel characteristics of char. *Waste Management*, **83**, 131–141.

Chanaka W., Veksha A., Giannis A., Lisak G. and Lim T. (2019b). Effects of sewage sludge organic and inorganic constituents on the properties of pyrolysis products, *Energy Conversion and Management,* **196,** 1410–1419.

Cortés A. and Bridgwater A. (2015). Kinetic study of the pyrolysis of miscanthus and its acid hydrolysis residue by thermogravimetric analysis. *Fuel Processing Technology*, **138**, 184–193.

Flynn J.H. (1997). The temperature integral its use and abuse. *Thermochimica Acta*, **300**(1), 83–92.

Font R., Fullana A. and Conesa J. (2005). Kinetic models for the pyrolysis and combustion of two types of sewage sludge. *Journal of Analytical and Applied Pyrolysis*, **74**, 429–438.

Furimsky E. and Sears P. (1988). Iron-catalyzed gasification of char in CO_2. *Energy & Fuels*, **2**, 634–639.

Gao N., Kamran K., Quan C. and Williams P.T. (2020). Thermo-chemical conversion of sewage sludge: A critical review. *Progress in Energy and Combustion Science*, **79**, 100843.

Gao N., Li J., Qi B., Li A., Duan Y. and Wang Z. (2014). Thermal analysis and products distribution of dried sewage sludge pyrolysis. *Journal of Analytical and Applied Pyrolysis*, **105**, 43–48.

García A., Ariza J., Martín J., Díaz J.A.I. and Morán A. (2009). Kinetic models based in biomass components for the combustion and pyrolysis of sewage sludge and its compost. *Journal of Analytical and Applied Pyrolysis*, **86**, 108–114.

Inguanzo M., Domínguez A., Menéndez J.A., Blanco C.G. and Pis J.J. (2002). On the pyrolysis of sewage sludge: the influence of pyrolysis conditions on solid, liquid and gas fractions. *Journal of Analytical and Applied Pyrolysis*, **63**, 209–222.

Ji A., Zhang S., Lu X. and Liu Y. (2010). A new method for evaluating the sewage sludge pyrolysis kinetics. *Waste Management*, *3***0**, 1225–1229.

Kacprzak M., Neczaj E., Fijalkowski K., Grobelak A., Grosser A., Worwag M., Rorat A., Brattebo H., Almas A. and Singh B.

(2017). Sewage sludge disposal strategies for sustainable development, *Environmental Research*, **156,** 39–46.

Karaca C., Sozen S., Orhon D. and Okutan H. (2018). High temperature pyrolysis of sewage sludge as a sustainable process for energy recovery. *Waste Management*, **78**, 217–226.

Karayildirim T., Yuksel M. and Bockhorn H. (2006). Characterisation of products from pyrolysis of waste sludges. *Fuel*, **85**, 1498–1508.

Li C. and Suzuki K. (2010). Tar property, analysis, reforming mechanism and model for biomass gasification–an overview. *Renewable & Sustainable Energy Reviews*, **13**, 594–604.

Morf P., Hasler P. and Nussbaumer T. (2002). Mechanisms and kinetics of homogeneous secondary reactions of tar from continuous pyrolysis of wood chips. *Fuel*, **81**, 843–853.

Neves D., Thunman H., Matos A., Tarelho L. and Gómez-Barea A. (2011). Characterization and prediction of biomass pyrolysis products. *Progress in Energy and Combustion Science*, **37**, 611–630.

Nowicki L. and Ledakowicz S. (2014). Comprehensive characterization of thermal decomposition of sewage sludge by TG–MS. *Journal of Analytical and Applied Pyrolysis*, **110**, 220–228.

Porada S. (2004). The reactions of formation of selected gas products during coal pyrolysis. *Fuel*, **83**, 1191–1196.

Rincón S., Mendoza L. and Gómez A. (2019). Tratamiento térmico de biosólidos para aplicaciones energéticas, Kassel University Press, Kassel–Germany.

Roedder E. (1959). Silicate melt systems. *Physics and Chemistry of the Earth*, **3**, 224–297.

Roskosch A. and Heidecke P. (2018). S*ewage sludge disposal in the Federal Republic of Germany, Technical Report*, German Environment Agency.

Sánchez M., Menéndez J., Domínguez A., Pis J., Martínez O., Calvo L. and Bernad P. (2009). Effect of pyrolysis temperature on the composition of the oils obtained from sewage sludge. *Biomass and Bioenergy*, **33**, 933–940.

Seggiani M., Vitolo S., Puccini M. and Bellini A. (2012). Cogasification of sewage sludge in an updraft gasifier, *Fuel*, **93**, 486–491.

Shao J., Yan R., Chen H., Yang H. and Lee D.H. (2010). Catalytic effect of metal oxides on pyrolysis of sewage sludge. *Fuel Processing Technology,* **91**, 1113–1118.

Tang S., Zheng C. and Zhang Z. (2018). Effect of inherent minerals sewage sludge pyrolysis: Product characteristics, kinetics and thermodynamics. *Waste Management,* **80**, 175–185.

Thipkhunthod P., Meeyoo V. and Rangsunvigit P. (2007). Rirksomboom, Describing sewage sludge pyrolysis kinetics by a combination of biomass fractions decomposition. *Journal of Analytical and Applied Pyrolysis*, **79**, 78–85.

Trinh T.N., Jensen P.A., Dam-Johansen K., Knudsen N.O. and Sorensen H.R. (2013). Influence of the pyrolysis temperature on the sewage sludge product distribution, bio-oil, and char properties, *Energy & Fuels*, **27**, 1419–1427.

Urban D. and Antal M. (1982). Study of the kinetics of sewage sludge pyrolysis using DSC and TGA. *Fuel*, **61**, 799–806.

Urych B. and Smolinski A. (2016). Kinetics of sewage sludge pyrolysis and air gasification of its chars. *Energy Fuels,* **30**, 4869–4878.

Van Soest P., Robertson J. and Lewis B. (1991). Methods for dietary fiber, neutral detergent fiber, and nonstarch polysaccharides in relation to animal nutrition. *Journal of Dairy Science*, **74**, 3583–3597.

Varhegy G., Antal M., Jakab E. and Szabo P. (2007). Kinetic modeling of biomass pyrolysis. *Fuel*, **86**, 1781–1788.

Wang L., Chang Y. and Li A. (2019). Hydrothermal carbonization for energy-efficient processing of sewage sludge: A review. *Renewable and Sustainable Energy Reviews*, **108**, 423–440.

Wesenbeeck S.V., Prins W., Ronsse F. and Antal Jr. M.J. (2014). Sewage sludge carbonization for biochar applications. *Fate of Heavy Metals, Energy & Fuels*, **28**, 5312–5326.

Wichelns D., Drechsel P. and Qadir M. (2015). Wastewater: Economic asset in an urbanizing world, in: Dreschel P., Qadir M. and Wichelns D. (Eds.), *Wastewater Economic Asset in an Urbanizing World*, Springer, Dordrecht, pp. 3–14.

Xu Q., Tang S., Wang J. and Ko J. (2018). Pyrolysis kinetics of sewage sludge and its biochar characteristics. *Process Safety and Environmental Protection*, **115**, 49–56.

Yang H., Yan R., Chen H., Ho Lee D. and Zheng C. (2007). Characteristics of hemicellulose, cellulose and lignin pyrolysis. *Fuel*, **86**, 1781–1788.

Zhu X., Zhao L., Fu F., Yang Z., Li F., Yuan W., Zhou M., Fang W., Zhen G., Lu X. and Zhang X. (2019). Pyrolysis of pre-dried dewatered sewage sludge under different heating rates: Characteristics and kinetics study. *Fuel*, **255**, 1–7.